Resonance Raman Studies of $[CpFe(CO)_2]_2$ and $[Cp^*Fe(CO)_2]_2$: A Probe of Photoreactive States and Intermediates

Marcello Vitale,[1a] Kayla K. Lee,[1a] Craig F. Hemann,[1b] Russ Hille,[1b] Terry L. Gustafson,*[,1a] and Bruce E. Bursten*[,1a]

Contribution from the Departments of Chemistry and Medical Biochemistry, The Ohio State University, Columbus, Ohio 43210

Received September 30, 1994[⊗]

Abstract: $[CpFe(CO)_2]_2$ (**1**: Cp = η^5-C_5H_5) and its permethylated analog $[Cp^*Fe(CO)_2]_2$ (**1***: Cp* = η^5-C_5Me_5) were examined using Raman and resonance Raman spectroscopy. Raman bands associated with high-energy C−O stretches and low-energy Fe−Fe and Fe−(μ-CO) are detected at a variety of excitation wavelengths. The assignments of the C−O stretches and the calculation of carbonyl force constants are presented. The resonance behavior of the C−O stretching modes in **1** and **1*** is correlated to their lower energy electronic absorption bands, and these results provide an indication of the molecular orbitals involved in the electronic transitions. The spectra show evidence for the formation of the CO-loss photoproducts $Cp_2Fe_2(\mu\text{-}CO)_3$ (**2**) and $Cp^*_2Fe_2(\mu\text{-}CO)_3$ (**2***). **2** and **2*** exhibit rich resonance Raman spectra, including a number of overtones and combination bands of the low-energy vibrational modes. Such spectra suggest a strong coupling between the Fe−Fe stretching and Fe−(μ-CO) breathing modes.

Introduction

The classic piano-stool dimer $[CpFe(CO)_2]_2$ (**1**: Cp = η^5-C_5H_5) continues to be among the most widely studied dinuclear organometallic complexes. **1** exhibits a rich photochemistry that is dominated by two very different photochemical channels, namely the loss of CO to form the paramagnetic triply-bridged intermediate $Cp_2Fe_2(\mu\text{-}CO)_3$ (**2**), and homolysis of the dimer into the mononuclear 17e· radicals ·$FeCp(CO)_2$ (**3**) (Scheme 1).[2,3] Recent attempts by several laboratories to refine better the detailed mechanistic aspects of Scheme 1 have uncovered an increasingly intricate web of photochemical reactions and transients following the initial irradiation of the molecule.[4] Most of these studies have involved vibrational spectroscopic detection, which will be the focus of this paper.

The infrared spectroscopy of **1**, especially in the high-energy C−O stretch region, has been intensely studied since the time of its initial synthesis.[5] IR spectroscopy of the carbonyl-stretch region proved that **1** was present in solution as a mixture of bridged trans and cis forms (**1t** and **1c**, respectively), in a ratio dependent on solvent polarity, together with very small amounts

Scheme 1

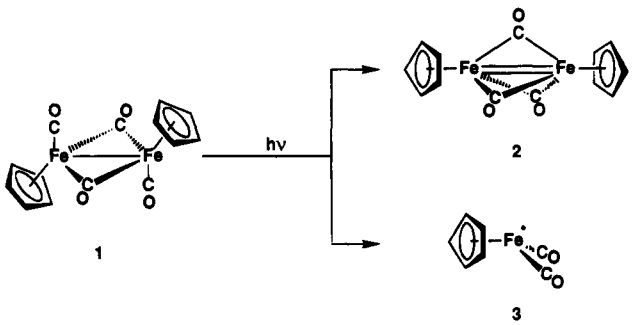

of the unbridged, all-terminal form **1u**, which is intermediate in the thermal cis-trans isomerization pathway (Scheme 2).[6] The more sterically hindered permethylated analog $[Cp^*Fe(CO)_2]_2$ (**1***: Cp* = η^5-C_5Me_5) appears to exist in solution, at equilibrium, exclusively as the trans isomer,[7] although the cis isomer has been observed as a short-lived, photogenerated species.[3k]

[⊗] Abstract published in *Advance ACS Abstracts*, February 15, 1995.

(1) (a) Department of Chemistry. (b) Department of Medical Biochemistry.

(2) (a) Meyer, T. J.; Caspar, J. V. *Chem. Rev.* **1985**, *85*, 187−218. (b) Baird, M. C. *Chem. Rev.* **1988**, *88*, 1217−27.

(3) (a) Wrighton, M. S.; Abrahamson, H. B. *J. Am. Chem. Soc.* **1977**, *99*, 5510−2. (b) Abrahamson, H. B.; Palazzotto, M. C.; Reichel, C. L.; Wrighton, M. S. *J. Am. Chem. Soc.* **1979**, *101*, 4123−7. (c) Tyler, D. R.; Schmidt, M. A.; Gray, H. B. *J. Am. Chem. Soc.* **1979**, *101*, 2753−5. (d) Caspar, J. V.; Meyer, T. J. *J. Am. Chem. Soc.* **1980**, *102*, 7794−5. (e) Hooker, R. H.; Mahmoud, K. A.; Rest, A. J. *J. Chem. Soc., Chem. Commun.* **1983**, 1022−4. (f) Tyler, D. R.; Schmidt, M. A.; Gray, H. B. *J. Am. Chem. Soc.* **1983**, *105*, 6018−21. (g) Hepp, A. F.; Blaha, J. P.; Lewis, C.; Wrighton, M. S. *Organometallics* **1984**, *3*, 174−7. (h) Moore, B. D.; Simpson, M. B.; Poliakoff, M.; Turner, J. J. *J. Chem. Soc., Chem. Commun.* **1984**, 972−4. (i) Dixon, A. J.; Healy, M. A.; Hodges, P. M.; Moore, B. D.; Poliakoff, M.; Simpson, M. B.; Turner, J. J.; West, M. A. *J. Chem. Soc., Faraday Trans. 2* **1986**, *82*, 2083−92. (j) Dixon, A. J.; Healy, M. A.; Poliakoff, M.; Turner, J. J. *J. Chem. Soc., Chem. Commun.* **1986**, 994−6. (k) Moore, B. D.; Poliakoff, M.; Turner, J. J. *J. Am. Chem. Soc.* **1986**, *108*, 1819−22. (l) Bursten, B. E.; McKee, S. D.; Platz, M. S. *J. Am. Chem. Soc.* **1989**, *111*, 3428−9.

(4) (a) Bloyce, P. E.; Campen, A. K.; Hooker, R. H.; Rest, A. J.; Thomas, N. R.; Bitterwolf, T. E.; Shade, J. E. *J. Chem. Soc., Dalton Trans.* **1990**, 2833−41. (b) Dixon, A. J.; George, M. W.; Hughes, C.; Poliakoff, M.; Turner, J. J. *J. Am. Chem. Soc.* **1992**, *114*, 1719−29. (c) Zhang, S.; Brown, T. L. *J. Am. Chem. Soc.* **1992**, *114*, 2723−5. (d) Zhang, S.; Brown, T. L. *J. Am. Chem. Soc.* **1993**, *115*, 1779−89. (e) McKee, S. D.; Krause, J. A.; Lunder, D. M.; Bursten, B. E. *J. Coord. Chem.* **1994**, *32*, 249−59. (f) Kvietok, F. A.; Bursten, B. E. *J. Am. Chem. Soc.* **1994**, *116*, 9807−8. (g) Moore, J. N.; Hansen, P. A.; Hochstrasser, R. M. *J. Am. Chem. Soc.* **1989**, *111*, 4563−6. (h) Anfinrud, P. A.; Han, C.-H.; Lian, T.; Hochstrasser, R. M. *J. Phys. Chem.* **1991**, *95*, 574−8.

(5) Piper, T. S.; Cotton, F. A.; Wilkinson, G. *J. Inorg. Nucl. Chem.* **1955**, *1*, 165−74.

(6) (a) Cotton, F. A.; Yagupsky, G. *Inorg. Chem.* **1967**, *6*, 15−20. (b) Fischer, R. D.; Vogler, A.; Noack, K. *J. Organomet. Chem.* **1967**, *7*, 135. (c) Noack, K. *J. Organomet. Chem.* **1967**, *7*, 151. (d) Manning, A. R. *J. Chem. Soc. A* **1968**, 1319−24. (e) Bullitt, J. G.; Cotton, F. A.; Marks, T. J. *J. Am. Chem. Soc.* **1970**, *92*, 2155−6. (f) McArdle, P.; Manning, A. R. *J. Chem. Soc. A* **1970**, 2133−6. (g) Bullitt, J. G.; Cotton, F. A.; Marks, T. J. *Inorg. Chem.* **1972**, *11*, 671−6. (h) Gansow, O. A.; Burke, A. R.; Vernon, W. D. *J. Am. Chem. Soc.* **1972**, *94*, 2550−2. (i) Adams, R. D.; Cotton, F. A. *Inorg. Chim. Acta* **1973**, *7*, 153−6. (j) Kirchner, R. M.; Marks, T. J.; Kristoff, J. S.; Ibers, J. A. *J. Am. Chem. Soc.* **1973**, *95*, 6602−13.

(7) King, R. B.; Bisnette, M. B. *J. Organomet. Chem.* **1967**, *8*, 287−97.

0002-7863/95/1517-2286$09.00/0

Scheme 2

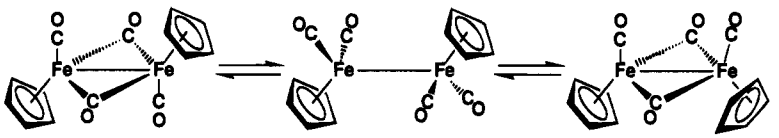

1t 1u 1c

The photochemical intermediates **2** and **3** are also readily detected via IR spectroscopy of the CO stretch region. At the concentrations used for our studies, the radicals **3** produced by homolysis have a half-life of about 25 μs in the absence of radical traps, i.e. under conditions in which they can react solely via radical recombination.[3d,k] On the other hand, the CO-loss product **2** is a long-lived intermediate for which the half-life has been reported to be 3 s.[3d,g,h] **2** exhibits a characteristic IR absorption at 1823 cm^{-1}, attributed to the E′ CO stretch vibrational mode of the D_{3h} $Fe_2(\mu\text{-}CO)_3$ core of the molecule. It also shows a diagnostic electronic absorption at 515 nm in both laser-flash-photolysis and matrix-isolation experiments. The Cp* analog $Cp^*_2Fe_2(\mu\text{-}CO)_3$ (**2***) is even more stable, and it has been isolated and characterized by X-ray crystallography.[8] The ground state of **2*** was found to be a triplet, in accord with the results of Fenske–Hall MO calculations carried out on **2**.

In view of the numerous detailed studies of **1** using infrared spectroscopy, it is surprising to find virtually no Raman spectroscopic studies of this molecule. San Filippo has reported a low-energy Raman spectrum of solid **1** and proposed that a band at 226 cm^{-1} could be attributed to the Fe–Fe stretch in the ground-state molecule.[9] Shriver reexamined the Raman spectrum of **1** and found no evidence for an Fe–Fe stretching mode.[10] To date, there have been no reports of the Raman spectrum of **1** in the carbonyl-stretch region.

We suspect that the scarcity of Raman studies of **1** and related dinuclear complexes is due to their photochemical reactivity, which, it might be believed, would render the molecules unsuitable for Raman investigation. However, Raman and resonance Raman spectroscopy are uniquely suited to provide detailed information about the way individual vibrational modes change on going from the ground state to the various excited states,[11] a relationship that we thought could be exploited to investigate the ground-state properties of both **1** and any photochemical products generated during the Raman experiment. We also hoped that the extreme sensitivity of resonance Raman spectroscopy could allow for the detection of low-concentration transient species with a much simpler experimental setup than required by the traditional techniques for the study of transients. In this paper, we report the Raman spectra of **1** and **1*** at a variety of excitation wavelengths. As will be detailed, we have found Raman bands that correspond to high-energy (>1700 cm^{-1}) CO stretches in **1** and to low-energy (ca. 200 cm^{-1}) vibrational modes due to the Fe–Fe stretch. We will also demonstrate the formation of photoproducts **2** and **2*** during the Raman experiments, species that are readily detected by resonance Raman spectroscopy.

Experimental Details

The irradiation wavelengths (λ_{irr}) used to collect Raman spectra were selected to cover a wide energy range, from red to UV and from off-resonance conditions to values within one or more of the absorption bands of **1** and **1***. A variety of laser systems were employed, which will be described briefly.

Light of 263 or 355 nm was obtained as the fourth or third harmonic, respectively, of a kilohertz mode-locked Nd:YLF laser (Coherent, Antares 76 YLF). Light of 566 nm was produced by a dye laser (Coherent, 702–2) using R6G (Exciton Corp.) as the excitation medium and DQOCI (Exciton Corp.) as the saturable absorber and pumped by the second harmonic (532 nm) of a megahertz mode-locked Nd:YAG laser (Coherent, Antares 76S). The lines at 457.9, 514.5, and 528.7 nm were from of a CW argon ion laser (Coherent, INNOVA 307). Light of 648 nm was produced by a DCM dye laser (Coherent, 599 Standing Wave) pumped by the above CW argon ion laser working in the multiline mode. Finally, 785 nm light was produced by a tunable Ti-sapphire laser (Coherent, 890), also pumped by the above argon ion laser.

The irradiation beam was focused onto a spinning quartz sample cell at an angle of ca. 45–60°. The back-scattered light was collected and dispersed through a single-stage spectrograph (ISA, THR 640 or Chromex 500IS 0.5 m), using 1200, 1800, or 3600 grooves/mm gratings. An interference filter was used, when available (at 457.9, 514.5, 648, and 785 nm; Kaiser Optical Systems), to block Raylegh scatter before the spectrograph. The signal was detected using a liquid N_2-cooled Charge Coupled Device (CCD; Photometrics CC200 System with a Thomson-CSF 576 × 384 chip or Princeton Instruments, LN/CCD-1024 TKB with a 1024 × 1024 chip). Data collection times varied widely depending on signal quality and intensity. At higher irradiation energies (λ < 457.9 nm), the sample had to be changed frequently because of photodegradation. At every irradiation wavelength, multiple data files were collected to check for possible degradation of the sample and to help eliminate spurious signal due to high-energy background radiation.

The detection systems were interfaced with IBM-compatible computers running locally-developed software based on the ASYST scientific package (Asyst Software Technologies) or the CCD Spectrometric Multichannel Analysis (CSMA) software version 2.2 provided by Princeton Instruments. The data were then transferred, in the form of ASCII files, to a scientific graphic program (Kaleidagraph, by Abelbeck Software, running on Apple Macintosh computers) to be worked up as described below. Band fitting was performed using PeakFit (Jandel Scientific), on IBM-compatible computers.

Infrared spectra were collected with a Nicolet Magna-IR 550 FT-IR spectrometer. A Cary 17-I UV/Vis/IR spectrometer, with digital modification by On Line Instrument Systems (OLIS), was used to obtain electronic spectra.

$[CpFe(CO)_2]_2$ (**1**) was synthesized according to the published procedure,[12] and $[Cp^*Fe(CO)_2]_2$ (**1***) was purchased from Strem Chemicals and used without further purification. Both compounds are air stable as solids, but their solutions are rapidly attacked by oxygen. The 2 mM solutions employed were therefore prepared and handled under an Ar atmosphere in a drybox (Innovative Technology, MB150). Cyclohexane (Aldrich, spectrophotometric grade) was a suitable non-coordinating solvent that would not interfere with the Raman spectral regions of interest. The solvent was degassed by numerous freeze–pump–thaw cycles before use. The sample cells were ~0.9 mm i.d. suprasil quartz tubes, containing about 1 mL of solution each, capped with recessed head silicone rubber Suba Seal septa (Aldrich) and parafilm.

Raman spectra were collected in two distinct energy ranges: the first was roughly centered around 1900 cm^{-1}, the second had a lower

(8) Blaha, J. P.; Bursten, B. E.; Dewan, J. C.; Frankel, R. B.; Randolph, C. L.; Wilson, B. A.; Wrighton, M. S. *J. Am. Chem. Soc.* **1985**, *107*, 4561–2.

(9) San Filippo, J.; Sniadoch, H. J. *Inorg. Chem.* **1973**, *12*, 2326–33.

(10) Onaka, S.; Shriver, D. F. *Inorg. Chem.* **1976**, *15*, 915–8.

(11) Myers, A. B.; Mathies, R. A. In *Biological Applications of Raman Spectroscopy.*; Spiro, T. G., Ed.; Wiley-Interscience: New York, 1987; Vol. 2.

(12) King, R. B. *Organomet. Synth.* **1965**, *1*, 114.

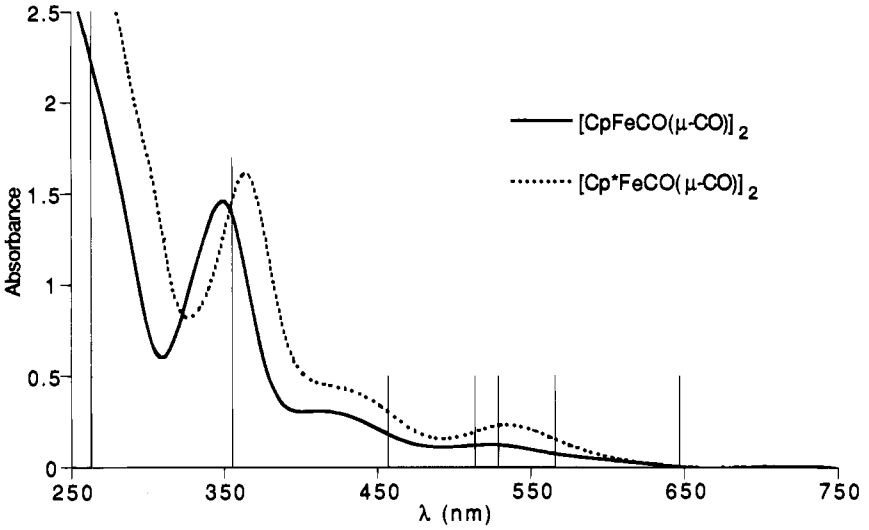

Figure 1. UV/vis spectra of **1** and **1***, (2.0 ± 0.1) × 10^{-4} M in cyclohexane; the thin vertical lines indicate the irradiation wavelengths at which Raman spectra were measured.

energy limit as close to the excitation position as allowed by the particular instrumental setup (notch filter cutoff or width of the Raylegh scatter).

To convert the abscissas of the Raman spectra from CCD-pixel number to wavenumber scale, standards were used for which some of the peak positions are known and tabulated. For each set of data collected in identical experimental conditions, spectra of a number of such standards, such as benzene, toluene, carbon tetrachloride, trichloroethylene, cyclohexane, and ethyl acetate, were also obtained. The wavenumber scale was then established by fitting a quadratic function to the resulting array of wavenumber vs pixel number pairs. In the case of the higher energy window examined, a lack of known and convenient peak positions in the region required the use of secondary standards. The positions of a large number of relatively weak features in the spectra of benzene, toluene, and cyclohexane were determined with a wide detection window that included more intense peaks of benzene, toluene, acetonitrile, and trichloroethylene. These were used to determine the wavenumber scale for narrower detection ranges. Because of these and other factors (*vide infra*), the indetermination in the reported peak positions is about ±2 cm^{-1}.

To obtain the Raman spectra presented here, a modified solvent spectrum was subtracted from the raw data. More precisely, the solvent spectra, obtained in the same experimental conditions as the sample spectra, had to be divided by a scaling factor, which ranged from a constant to a quadratic expression, followed by the addition of an offset term, which also varied from a constant to a fourth-order polynomial. Such mathematical manipulations were made necessary by the strong absorbance of the samples at most of the irradiation wavelengths, resulting in different amounts of light being diffracted and different imaging of the diffracted light onto the CCD chip. The problem was most pronounced for data collected without an interference filter to block Rayleigh scatter. An apparent jitter of the image of the refracted light onto the CCD chip was also observed, so that the wavenumber scales of different spectra usually differed by a non-integer pixel offset.

Subtraction of the solvent spectrum gave generally satisfying results in the CO stretch region, where cyclohexane presents only very weak structures that have intensity comparable to that of the peaks observed for **1** or **1*** under off-resonance conditions. However, cyclohexane presents relatively intense bands at 383.5 and 425.9 cm^{-1} and very intense bands at 801 and 1027.4 cm^{-1}. Due to the factors pointed out above, positive and negative residuals of the cyclohexane peaks are present in many of the spectra shown for this energy region and make difficult, at times, the identification of overlapping bands of the samples.

Results

In order to assure that both off-resonance and resonance Raman spectra are obtained, a variety of Raman excitation wavelengths were used. Figure 1 shows the solution electronic absorption spectra of **1** and **1***, with the various wavelengths of λ_{irr} displayed as vertical bars on the abscissa. Note that the spectrum of **1*** is slightly red-shifted relative to that of **1**, although this shift is not expected to have a major effect on the Raman scattering. The lowest energy excitation wavelength shown, 647 nm, is off-resonance for both **1** and **1***; the other excitation wavelengths are capable of exciting different electronic transitions in the molecules.

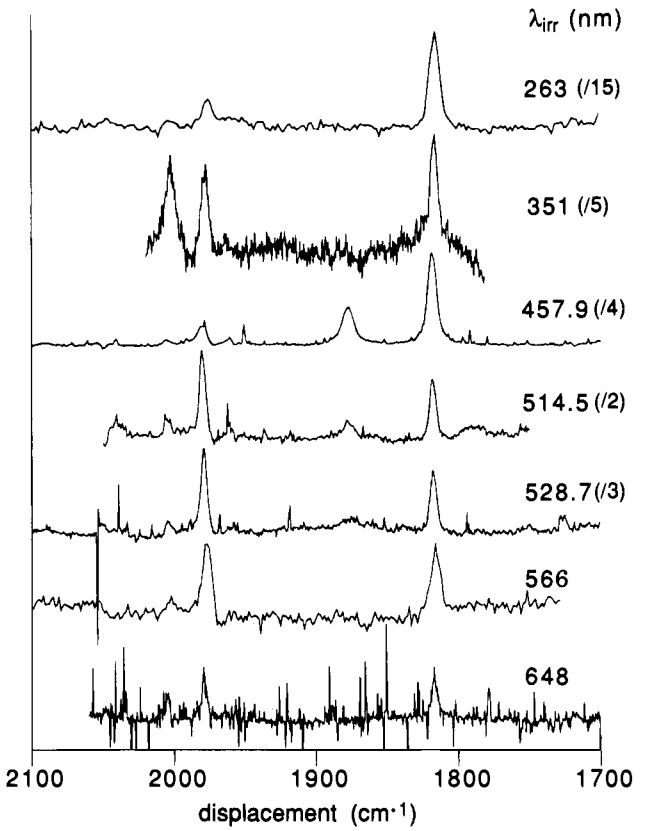

Figure 2. Raman spectra of cyclohexane solutions of **1** in the CO stretch region, normalized on the 1973 cm^{-1} peak of the solvent. The scale factors in parentheses make the spectra of comparable size.

High-Energy Vibrations. The Raman spectra obtained for **1** in the 1700−2100 cm^{-1} region are shown in Figure 2. This region is, of course, the expected one for C−O stretching modes, and prominent bands are present that are at consistent frequencies for coordinated CO ligands. At all irradiation wavelengths,

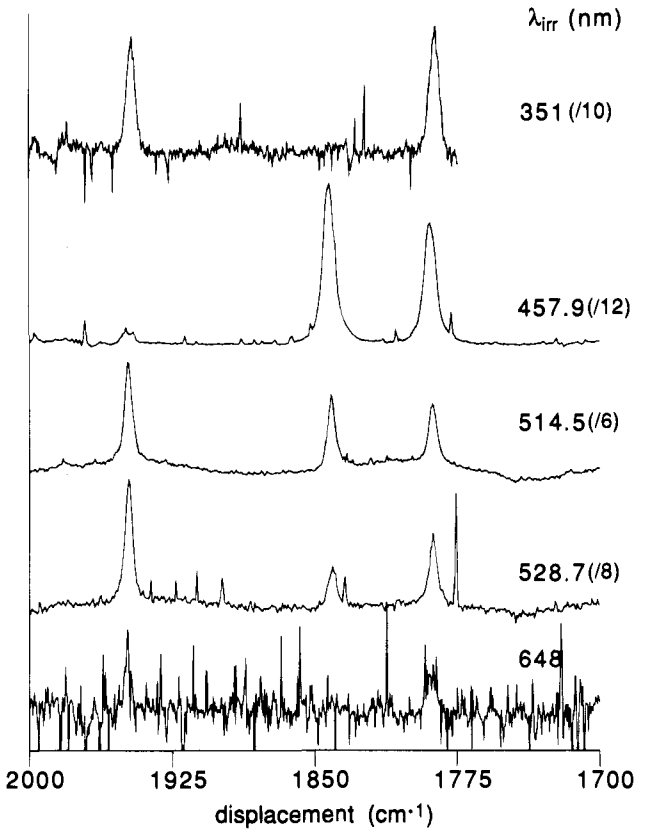

Figure 3. Raman spectra of cyclohexane solutions of **1*** in the CO stretch region, normalized on the 1973 cm^{-1} peak of the solvent. The scale factors in parentheses make the spectra of comparable size.

two bands are apparent, at 1818 and 1979 cm^{-1}, their energy being constant within experimental error. A third, usually weaker, band at 2004 cm^{-1} can be identified in all of the spectra shown, most clearly those with λ_{irr} = 648 and 351 nm.[13] Finally, an additional band, at 1877 cm^{-1}, is present only in the spectra for which λ_{irr} = 528.7, 514.5, and 457.9 nm. As will be discussed, this band is assigned to the symmetric A_1' (under D_{3h}) C−O stretching mode of photogenerated **2**.

Figure 3 presents the equivalent results for the case of the Cp* analog **1***. Two bands, at 1948 and 1788 cm^{-1}, are observed at every λ_{irr}. A third band, at 1841 cm^{-1}, is visible, and even dominant, in the spectra obtained with 528.7, 514.5, and 457.9 nm laser light; this band is attributed to the CO-loss product **2***. The shift of the CO stretching modes to lower energy in the Cp* complexes **1*** and **2*** relative to the Cp complexes **1** and **2** is consistent with the IR spectra of the compounds and can be attributed to the greater donor ability of the Cp* ligands.

The spectra in Figures 2 and 3 were normalized by setting the area of the 1973 cm^{-1} peak of cyclohexane to unity (the factors noted in the figures were used there for the sole purpose to make the normalized spectra of comparable size). Each peak was fitted by a Voigt function (convolution of a Lorentzian and a Gaussian function), which accounts for both homogeneous and inhomogeneous dephasing pathways. The intensity of each band was measured as the area of the resulting Voigt fit. These results are shown numerically in Table 1, and graphically in Figure 4 in the form of excitation profiles from 648 to 351 nm. Of the peaks that are present at all irradiation wavelengths, those at 1979 cm^{-1} (of **1**) and at 1948 cm^{-1} (of **1***) have similar excitation profiles, as do those at 1818 cm^{-1} (of **1**) and at 1788 cm^{-1} (of **1***). The bands of the first pair reach an intensity maximum at 528.7 nm and become smaller at 457.9 nm and, finally, more intense at 351 nm. A roughly equivalent behavior is observed for the much less intense band of **1** at 2004 cm^{-1}. The bands of the second pair, the lowest energy carbonyl vibrations of **1** and **1***, appear to increase in intensity less than the corresponding higher energy bands in going from λ_{irr} = 648 to 528.7 nm, but they grow much larger at 457.9 nm.

The additional bands at 1877 and 1841 nm, assigned to **2** and **2***, respectively, are much more intense with 457.9 nm than with either 528.7 or 514.5 nm excitation. Moreover, the ratio between the intensity of these bands and that of the other observed peaks was found to be a function of irradiation light intensity, the additional bands being relatively stronger at higher laser power. Spectra collected with different accumulation times showed the additional peaks growing (relative to both the solvent and the other sample bands) at very short times, reaching a maximum after about 30 s with 110 mW of 457.9 nm light and finally reaching a stationary level somewhat lower than the maximum one. As will be discussed below, the behavior of these bands supports their assignment to Raman transitions of photochemically generated **2** and **2***.

Low-Energy Vibrations. The Raman spectra obtained for **1** and **1*** in the lower energy vibrational range are presented in Figures 5 and 6, respectively.[14] The observed peak positions are reported in Table 2. The intensities of the various spectra were, as in the case of those in the higher energy range, normalized on a solvent band, namely the peak at 425.9 cm^{-1}. A large spectral variation with irradiation wavelength is apparent. In particular, for **1**, the lowest frequency band observed is at 225 cm^{-1} when λ_{irr} is 647 or 351 nm, but at 214 cm^{-1} with irradiation light of 514.5, 457.9, or 263 nm. The Raman spectrum of **1*** with λ_{irr} = 647 or 514.5 nm exhibits its lowest-energy mode at 140−150 cm^{-1}.

All the low-energy bands in Figures 5 and 6 could be divided into two sets, based on their different dependence on laser light intensity. In particular, many of the bands observed with 528.7, 514.5, and 457.9 nm irradiation behaved much like the 1877 and 1841 cm^{-1} peaks present in the CO stretch region, their intensity depending nonlinearly on irradiation power. In the low-energy region, however, many bands of the two sets overlap each other, making their identification more difficult.

To address this problem, we compared spectra at two different light intensities, namely a "low"-intensity spectrum with 10 mW laser power and a "high"-intensity spectrum with 100 mW power. After normalizing the spectra on the area of a solvent peak, the difference between them included only the power-dependent bands. Such difference spectra at 514.5 nm are shown in Figures 7 and 8 for **1** and **1***, respectively. It is apparent that, at this irradiation wavelength, most of the bands are power dependent. This behavior is also observed for most of the bands visible for λ_{irr} = 528.7 and 457.9 nm.

Although the presence of some bands that are not power dependent is evident even in the 514.5 nm spectra (compare Figures 7 and 8 with the 514.5 nm spectra in Figures 5 and 6), the spectra including them alone, i.e. the complement of Figures 7 and 8, are exceedingly noisy. The same is the case for the data obtained with λ_{irr} = 528.7 nm, making it impossible to obtain a reliable excitation profile for the low-energy bands. Nevertheless, it is possible to derive reliable peak positions, and these are included in Table 2.

(13) The unusual intensity of the 2004 cm^{-1} band in the spectrum shown for 351 nm irradiation is doubtful because of an overlapping, and unfortunately very reproducible, sharp feature in the background at such λ_{irr}, due to either the solvent or our particular experimental setup.

(14) The spectrum of **1** at λ_{irr} = 351 nm is constructed from two spectra obtained at different grating positions; unfortunately, there is a gap between the two windows at about 490 cm^{-1}.

Table 1. Raman Intensities of C−O Stretches in **1** and **1***

compound	energy (cm^{-1})	intensity[a] for λ_{irr} (nm) values listed here						
		648	566	528.7	514.5	457.9	351	263
$Cp_2Fe_2(CO)_2(\mu\text{-}CO)_2$ (**1**)	2004	0.013 ± 0.002	0.04 ± 0.02	0.028 ± 0.008	0.023 ± 0.007	0.03 ± 0.01	0.35 ± 0.03	0.21 ± 0.05
	1979	0.030 ± 0.003	0.091 ± 0.007	0.220 ± 0.009	0.149 ± 0.007	0.12 ± 0.01	0.42 ± 0.03	0.54 ± 0.05
	1877			0.03 ± 0.01	0.049 ± 0.006	0.31 ± 0.04		
	1818	0.040 ± 0.003	0.09 ± 0.01	0.21 ± 0.01	0.144 ± 0.006	0.57 ± 0.05	0.68 ± 0.05	2.1 ± 0.1
$Cp^*_2Fe_2(CO)_2(\mu\text{-}CO)_2$ (**1***)	1948	0.030 ± 0.006		0.72 ± 0.02	0.45 ± 0.05	0.14 ± 0.03	0.92 ± 0.04	
	1841			0.24 ± 0.02	0.29 ± 0.02	2.18 ± 0.06		
	1788	0.039 ± 0.007		0.43 ± 0.02	0.29 ± 0.02	1.69 ± 0.06	1.04 ± 0.07	0.5 ± 0.2

[a] Intensities are relative to the 1973 cm^{-1} band of cyclohexane.

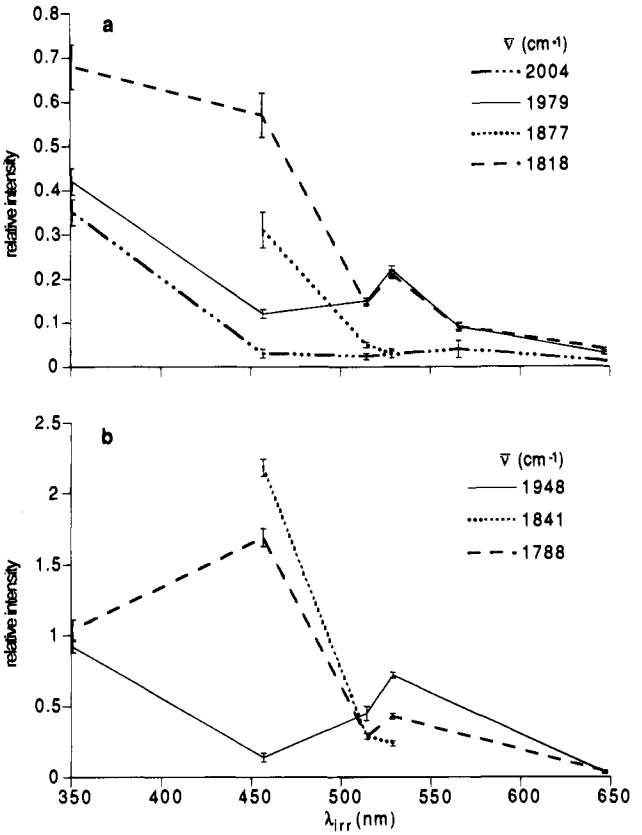

Figure 4. Resonance profiles of the CO stretches of **1** (a) and **1*** (b). The error bars are obtained from the standard deviation of the Voigt fit of the Raman bands.

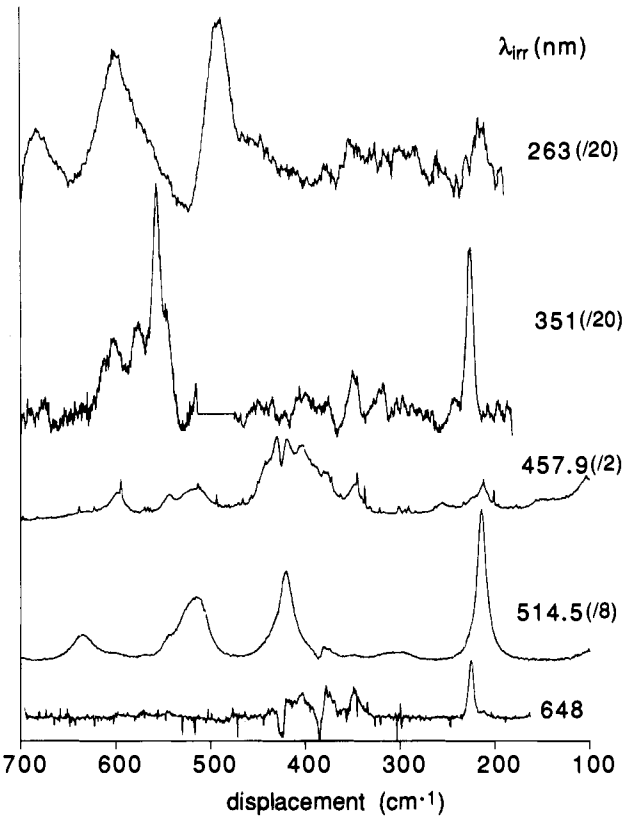

Figure 5. Raman spectra of cyclohexane solutions of **1** in the low-energy region, normalized on the 425.9 cm^{-1} peak of the solvent. The scale factors in parentheses make the spectra of comparable size.

Discussion

High-Energy Vibrations of 1 and 1*. As is typical for metal−carbonyl complexes, prior IR spectroscopic studies of **1** and **1*** have focussed primarily on the CO stretch region, with very little attention given to the low-energy vibrational modes. These previous studies, in conjunction with group theory, provide an easy basis on which to analyze the Raman spectra of the CO stretch region, and we will therefore first focus our discussion on these high-energy bands, which are presented in Figures 2 and 3.

As noted in the Introduction, **1** exists in solution as an equilibrium mixture of the trans and cis isomers **1t** and **1c** with C_{2h} and C_{2v} point symmetry, respectively.[6] For each isomer there are four normal vibrational modes that are essentially pure carbonyl stretches, because of the large energy difference between them and the other fundamentals. Moreover, the CO(bridging)−CO(terminal) coupling in these compounds has been found to be negligible, in first approximation, with respect to the CO(terminal)−CO(terminal) or the CO(bridging)−CO(bridging) interactions.[15] The comparison of the IR and Raman spectra supports this lack of coupling between bridging and terminal carbonyls. Therefore, the four modes for each isomer partition themselves into two pairs of symmetric (S) and antisymmetric (AS) combinations, one pair each for the terminal carbonyl stretches and for the bridging carbonyl stretches. Based on the well-founded assumption that the interaction force constants are positive,[16] the symmetric modes are expected to occur at higher energy than their antisymmetric counterparts.

In the case of the C_{2v} isomer **1c**, the four modes span the A_1 (S), B_1 (AS), and B_2 (AS) irreducible representations and all are therefore both IR and Raman active. On the other hand, the normal modes of the centrosymmetric trans isomer **1t**, which has C_{2h} symmetry, are neatly divided into two IR-active modes, of B_u (AS) and A_u (AS) symmetry, and two Raman-active modes, both of A_g (S) symmetry. With reference to the assignment of Bullitt, Cotton, and Marks for the IR bands of **1t** and **1c**,[6g] the identification of the corresponding Raman peaks is immediate. The IR and Raman peak positions in cyclohexane and their assignments are summarized in Table 3. The nonpolar solvent favors the trans isomer **1t** over cis **1c**, explaining why

(15) Bullitt, J. G.; Cotton, F. A. *Inorg. Chim. Acta* **1971**, *5*, 637−42.
(16) Cotton, F. A.; Kraihanzel, C. S. *J. Am. Chem. Soc.* **1962**, *84*, 4432−8.

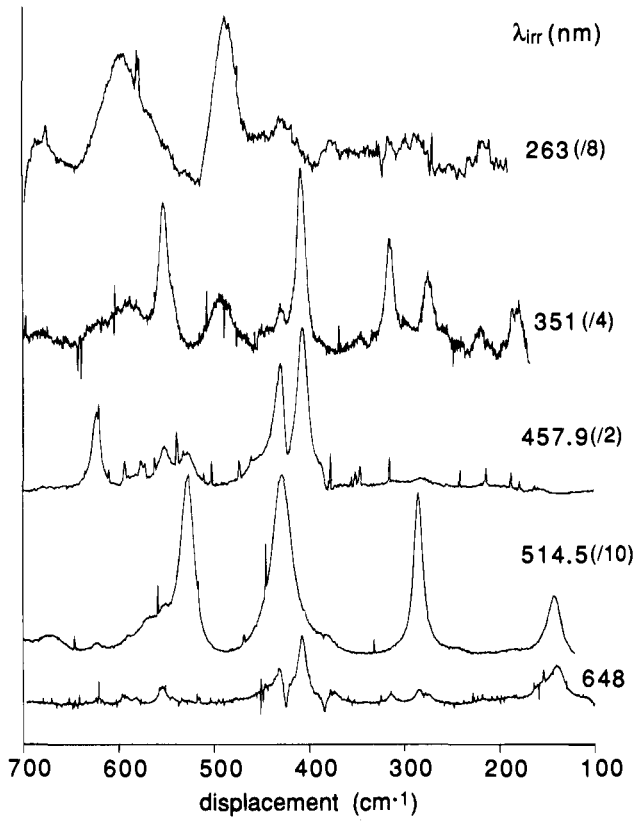

Figure 6. Raman spectra of cyclohexane solutions of **1*** in the low-energy region, normalized on the 425.9 cm^{-1} peak of the solvent. The scale factors in parentheses make the spectra of comparable size.

the weak A_1 combination of the bridging carbonyls in **1c** is not observed in the IR spectrum.

The energies of the bridging carbonyl stretches in the two isomers are nearly identical. As a matter of fact, just one band corresponding to a bridging carbonyl stretch is observed in either the IR or the Raman spectrum, the bands of **1t** and **1c** overlapping in both cases. From this observation it is clear that the CO(bridging)−CO(bridging) interactions are essentially the same in the two isomers. By contrast, the cis isomer shows a larger interaction between the terminal CO stretches than does the trans isomer; the symmetric combinations appear at widely different energies (2004 cm^{-1} for **1c** vs 1979 cm^{-1} for **1t**) whereas the antisymmetric modes are coincident at 1960 cm^{-1}. The B_2 AS mode of **1c**, which should be both IR and Raman active, is not observed in the Raman spectra.

Even more straightforward is the identification of the peaks in the high-energy region of the Raman spectrum of **1*** (Figure 3), which, for steric reasons, is present in solution only as the thermodynamically favored trans isomer. As can be seen in Table 3, the Raman bands of **1*** are shifted by nearly the same energy from their corresponding IR bands as they are for **1t**, i.e. $\Delta E(S - AS) = 19$ and 27 cm^{-1} for the terminal and bridging CO ligands, respectively.

Under the assumption that the interaction between terminal and bridging carbonyls is negligible, it is a simple matter to derive relevant bond and interaction force constants for the two types of CO ligands. Each pair of S/AS frequencies must satisfy the relationship

$$4\pi^2\nu^2 = (k \pm k_i)/\mu_{CO}$$

where ν is the vibrational frequency, μ_{CO} is the carbonyl reduced mass, k is the bond force constant, and k_i is the interaction force constant between the terminal or the bridging carbonyls; the plus sign applies to the symmetric modes and the minus sign to the antisymmetric ones.[17] The calculated values of k and k_i are presented in Table 4. The values of the force constants for **1c** are in excellent agreement with those reported previously by Bullitt and Cotton.[15] Those for **1t** and **1*** could not be derived prior to obtaining the Raman spectra because the symmetric stretching modes of these C_{2h} molecules are IR forbidden.

Table 2. Low-Energy Raman Peak Positions[a]

compound	peak positions for λ_{irr} (nm) values listed here					
	648	528.7	514.5	457.9	351	263
$Cp_2Fe_2(CO)_2(\mu\text{-}CO)_2$ (**1**)	225	*b*	214[c]	213[c]	226	214
	348	514[c]	227	224 sh	348	256
	403	543	302[c]	256	557	350
		633[c]	348	347	576	377
		723[c]	420[c]	405 sh	602	490
			440	420 sh[c]		598
			514[c]	514[c]		680
			545	543		
			572	598		
			600	631 sh[c]		
			632[c]	848 sh[c]		
			729[c]	916		
			843[c]	1115		
			935[c]			
$Cp^*_2Fe_2(CO)_2(\mu\text{-}CO)_2$ (**1***)	140	*b*	142[c]	284[c]	181	215
	154 sh	285[c]	285[c]	408	219	285
	275 sh	424 sh	426	431[c]	274	428
	284	430[c]	430[c]	530[c]	315	487
	314	528[c]	528[c]	554	408	597
	407	553	553	624	430	
	430 sh	570 sh[c]	570[c]	856[c]	492	677
	554	623	624	1115	552	
		672[c]	670[c]			
		713[c]	713[c]			
		818[c]	816[c]			
		853[c]	854[c]			
			955[c]			

[a] Peak positions in cm^{-1}; sh = shoulder. [b] Because of the absence of an interference filter, reliable spectroscopic data could not be obtained at this wavelength, below 450 cm^{-1} for **1** and 200 cm^{-1} for **1***. [c] Peaks that have been found to exhibit nonlinear dependence on light intensity in the 528.7, 514.5, and 457.9 nm spectra.

Identification of 2 and 2* in the Raman Experiment. Up to this point, we have been able to assign all the peaks observed in the CO stretch region of **1** and **1*** in off-resonance conditions, and we have accounted for every expected vibrational mode. The additional bands, present at 1877 and 1841 cm^{-1} in the spectra of **1** and **1***, respectively, collected with 528.7, 514.5, and 457.9 nm irradiation light, cannot therefore be attributed to **1** or **1***. Moreover, the power and time dependence of these bands suggest that they originate from photogenerated species. Such compounds must be unstable enough to return to starting material in, at most, minutes, since control IR spectra collected at the end of the Raman experiments indicated little or no decomposition. However, they must live long enough to increase in concentration for about 30 s, as indicated by the irradiation time dependence, before achieving a photostationary state in the closed system of the rotating cell.

As described in the Introduction, two different photochemical processes have been observed for **1** and **1***, namely homolysis and CO loss, yielding respectively the short-lived radicals **3** and **3*** or the long-lived, triply-bridged dimers **2** and **2*** (Scheme 1). Neither the observed band positions nor their temporal behavior are consistent with the radicals, which have a half-

(17) (a) Wilson, E. B., Jr.; Decius, J. C.; Cross, P. C. *Molecular Vibrations*; McGraw-Hill: New York, 1955. (b) Cotton, F. A. *Chemical Applications of Group Theory*, 3rd ed.; Wiley-Interscience: New York, 1990.

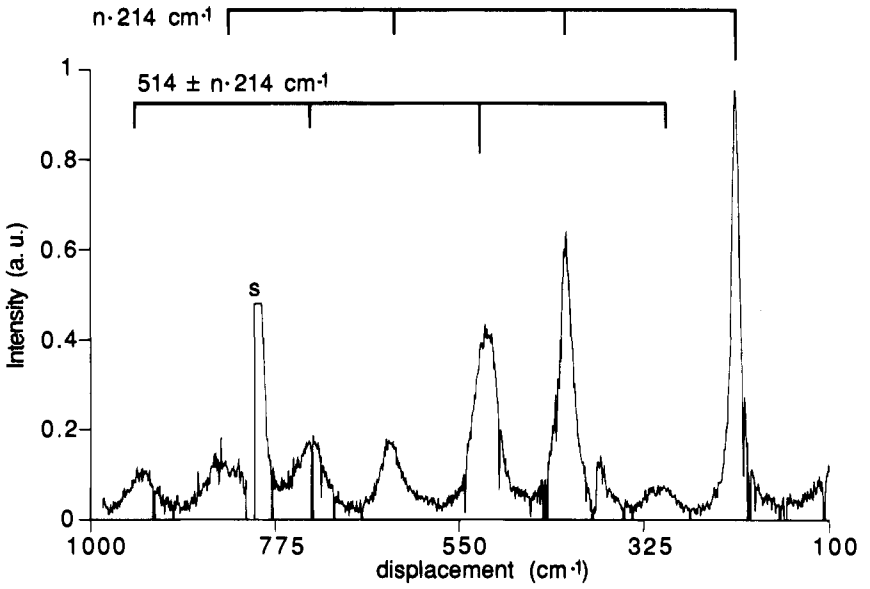

Figure 7. Raman spectrum of **2** in the low-energy region at λ_{irr} = 514.5 nm, obtained as the power-dependent component of the spectrum of a cyclohexane solution of **1**. The overhead rulers indicate overtones and combination bands deriving from the lowest-energy fundamental vibration. The peak marked "s" is due to the residual of the 801 cm^{-1} band of cyclohexane.

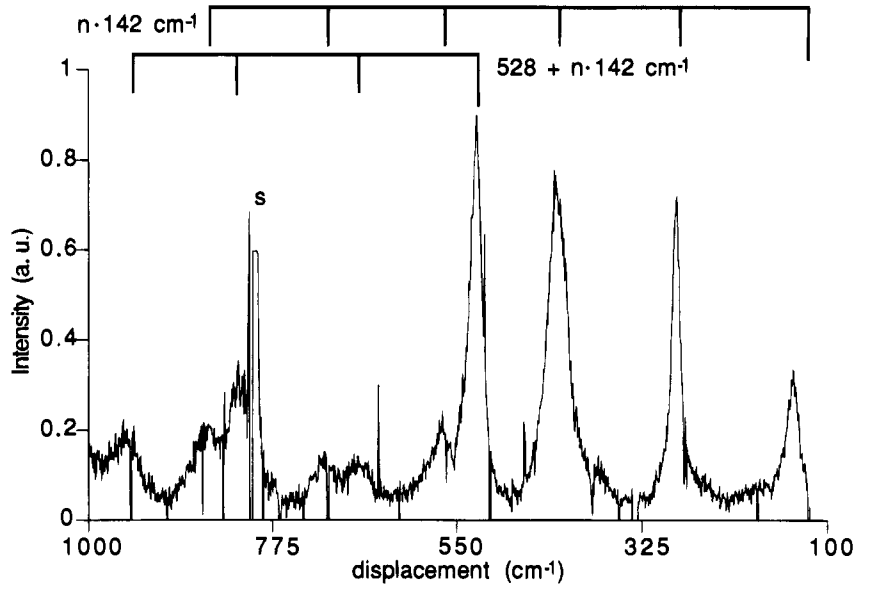

Figure 8. Raman spectrum of **2*** in the low-energy region at λ_{irr} = 514.5 nm, obtained as the power-dependent component of the spectrum of a cyclohexane solution of **1***. The overhead rulers indicate overtones and combination bands deriving from the lowest-energy fundamental vibration. The peak marked "s" is due to the residual of the 801 cm^{-1} band of cyclohexane.

life of about 25 μs[3d,k] and IR bands at 2004 and 1938 cm^{-1} [3h] for **3** and at 1984 and 1915 cm^{-1} [3k] for **3***. The single Raman peaks detected, at 1877 cm^{-1} in the spectrum of **1** and 1841 cm^{-1} in the spectrum of **1***, are more typical of bridging carbonyl stretches. Indeed, these bands are at just the expected energy for the symmetric counterparts of the IR-active E′ (under D_{3h}) modes of **2** and **2***. The IR band of **2** is observed at 1823 cm^{-1} [3h] and that of **2*** exhibits the expected shift to lower energy, 1790 cm^{-1},[3k] that accompanies the replacement of Cp by Cp*. The symmetric A_1' mode is expected to occur at higher energy than the antisymmetric E′ modes, and the Raman spectra indicate a consistent shift of ca. 50 cm^{-1} to higher energy relative to the IR-active bands (Table 3).

The assignment of the 1877 and 1841 cm^{-1} Raman bands to **2** and **2*** is supported by other observations. The generation and spectroscopic observation of a photoproduct is expected to be a two-photon process, namely one photon to generate the product and one to observe Raman scattering. Thus, the Raman scattering intensity of a photoproduct such as **2** is expected to be a nonlinear function of the excitation intensity, as is observed for the bands in question.[18] Further, transient UV/vis absorption spectra of **2** and **2*** show intense and broad absorption bands centered at 510–515 nm, whereas the radical products of homolysis show higher energy absorption, around 400 nm.[31] Thus, although the irradiation wavelengths of 528.7, 514.5, or 457.9 nm are energetic enough to form both radicals **3** and triply-bridged intermediates **2**, these wavelengths will be in resonance only with the latter. Resonance enhancement is necessary to explain the intensity observed for the photoproduct bands, especially when compared to the intensities of the bands of **1** and **1*** present in the same spectra. We believe that these observations, in conjunction with the energies of the CO stretching modes, provide overwhelming evidence that the 1877

(18) The Raman intensities of bands due to **2** and **2*** are not simple quadratic functions of the excitation intensity, as might be expected for a two-photon process, because of the long lifetimes of **2** and **2***.

Table 3. Band Positions and Assignments for the Carbonyl Stretching Modes[a]

$Cp_2Fe_2(CO)_2(\mu\text{-}CO)_2$					$Cp^*_2Fe_2(CO)_2(\mu\text{-}CO)_2$		
energy (cm^{-1})	trans (C_{2h}, **1t**)		cis (C_{2v}, **1c**)		energy (cm^{-1})	trans (C_{2h}, **1***)	
	Raman	IR	Raman	IR		Raman	IR
terminal					terminal		
2004			A_1	A_1			
1979	A_g				1948	A_g	
1960		B_u		B_2	1929		B_u
bridging					bridging		
1818	A_g		A_1		1788	A_g	
1792		A_u		B_1	1761		A_u

$Cp_2Fe_2(\mu\text{-}CO)_3$ (**2**)[b]			$Cp^*_2Fe_2(\mu\text{-}CO)_3$ (**2***)[b]		
energy (cm^{-1})	Raman	IR	energy (cm^{-1})	Raman	IR
bridging			bridging		
1877	A_1'		1841	A_1'	
1823[c]		E′	1790[d]		E′

[a] Room temperature cyclohexane solutions. [b] Symmetry labels for **2** and **2*** refer to the D_{3h} point group that describes the $Fe_2(\mu\text{-}CO)_3$ core. [c] From ref 3h. [d] From ref 3k.

Table 4. Carbonyl Stretching Force Constants

compd	terminal		bridging	
	k[a]	k_i[a]	k[a]	k_i[a]
$Cp_2Fe_2(CO)_2(\mu\text{-}CO)_2$				
trans, **1t**	15.66	0.14	13.17	0.20
cis, **1c**	15.87	0.35	13.17	0.20
$Cp^*_2Fe_2(CO)_2(\mu\text{-}CO)_2$ (**1***)	15.16	0.13	12.70	0.18
$Cp_2Fe_2(\mu\text{-}CO)_3$ (**2**)			13.69	0.27
$Cp^*_2Fe_2(\mu\text{-}CO)_3$ (**2***)			13.19	0.25

[a] k: C−O bond force constant. k_i: terminal−terminal or bridging−bridging interaction force constant; in mdyn/Å, ±0.03. For calculation, see text.

and 1841 cm^{-1} bands are due to photogenerated **2** and **2***, respectively.

The inability to observe the bands due to **2** (or **2***) at irradiation wavelengths outside of a relatively narrow window may be due to several reasons. First, it seems likely that the species exists in very low concentration relative to **1** (or **1***). Therefore the species would not be observed in the off-resonance spectra with λ_{irr} = 648, 351, or 263 nm, even though the latter two wavelengths are certainly energetic enough to cause CO loss. Moreover, the further photoreactivity of **2** and **2*** at the shorter irradiation wavelength could reduce the concentration of these transients in the photostationary state. The 566 nm irradiation might be expected to overlap significantly enough with the absorption band of **2** to lead to some resonance enhancement. However, 566 nm light may be below the energetic threshold for CO loss,[3i,4a,g,h] which means that very little **2**, if any, is produced at this λ_{irr}.

As was the case for **1** and **1***, we can assume that the CO stretches of **2** and **2*** are not coupled to any other vibrational modes. Under the D_{3h} symmetry of the $Fe_2(\mu\text{-}CO)_3$ core of the molecule, the vibrational frequencies depend on only two force constants, the C−O bond force constant, k, and the interaction force constant between the carbonyl dipoles, k_i: the frequency of the Raman-active A_1' vibrational mode is proportional to $(k + 2k_i)$, and the frequency of the IR-active E′ mode is proportional to $(k - k_i)$.[17] As based on the frequencies in Table 3, the calculated values of k and k_i for **2** and **2*** are given in Table 4. As expected, the value of k is considerably smaller for **2*** than for **2**, although the interaction constants of the two systems are very similar.

Analysis of the Excitation Profiles. Because Raman spectroscopy involves electronic excitation of the ground-state molecule, the analysis of the wavelength dependence of the Raman scattering intensity can provide valuable information about the relationship between the ground state (GS) and excited states (ES). In Figure 4, the Raman intensities for the spectra in Figures 2 and 3 are presented as excitation profiles, which are plots of the intensities as a function of λ_{irr}. We can interpret these profiles in the framework of Albrecht's theory,[19] in which resonance Raman intensities are described as the sum of two terms. For a given normal vibrational mode, Albrecht's *B* term is proportional to the extent of vibronic mixing induced by the mode between the resonant ES (denoted ES′) and other excited states of appropriate symmetry. Because all of the relevant Raman bands in the CO stretch region of **1** and **1*** have been assigned to totally symmetric modes (Table 3), this *B* term is expected to be small in the absence of degenerate ES.[11,19c,20]

The dominant contribution to the resonance enhancement of the intensity of totally symmetric modes comes, instead, from Albrecht's *A* term. The term is dependent on the electronic transition moment from the GS to ES′, explaining the general tendency, observed in Figure 4, for the excitation profiles to roughly reproduce the optical spectrum. Similarly, the greater intensity of the CO stretching bands of **1*** relative to those of **1** (cf. Figures 4a and 4b) can be directly related to the greater absorption coefficient of the former at all energies within the near-UV and visible regions.

Most important, the Raman scattering tensor is proportional to factors of the type

$$\langle \mathbf{i}|\mathbf{v}\rangle\langle \mathbf{v}|\mathbf{j}\rangle$$

where **i** and **j** are respectively the initial and final vibrational quantum numbers in the GS and **v** is a vibrational quantum number close to resonance in ES′.[11] These factors do not vanish for $\mathbf{i} \neq \mathbf{j}$ because of the difference in the vibrational wave functions of the GS and ES′, and they are larger the more the vibrational wave functions differ in equilibrium position, frequency, or composition. Thus, those vibrational modes involving bonds that are most affected in going from the GS to ES′, and that, therefore, are most involved in the initial path of distortion of the excited state, will see the greatest increase in their Raman scattering intensity.

Within this framework, the excitation profiles of Figure 4 can yield very important information about the nature of the lowest energy electronic transitions observed in the absorption spectra of **1** and **1***. Most notably, the terminal CO stretching modes have distinctly different excitation profiles than those of the bridging CO modes. The former are more enhanced when λ_{irr} falls within the first absorption band (566, 528.7, 514.5 nm), their intensity actually decreasing at the irradiation wavelength corresponding to the second absorption band (457.9 nm). The opposite is true for the bridging CO modes, which are much more enhanced in the second than the first absorption band. They are, moreover, less enhanced in the first absorption band than the terminal carbonyls.

These results indicate that the terminal and bridging C−O bonds are affected in different ways by excitation into the lowest energy ES′s. As is usual in the discussion of transition metal carbonyl complexes, variations in the C−O stretching force constant are closely linked to the CO π^* electron density, that is to the amount of π back-donation from the metal to the

(19) (a) Albrecht, A. C. *J. Chem. Phys.* **1961**, *34*, 1476−84. (b) Tang, J.; Albrecht, A. C. In *Raman Spectroscopy*; Szymanski, H. A., Ed.; Plenum Press: New York, 1970; Vol. 2. (c) Strommen, D. P.; Nakamoto, K. *J. Chem. Educ.* **1977**, *54*, 474−8.

(20) Inagaki, F.; Tasumi, M.; Miyazawa, T. *J. Mol. Spectrosc.* **1974**, *50*, 286−303.

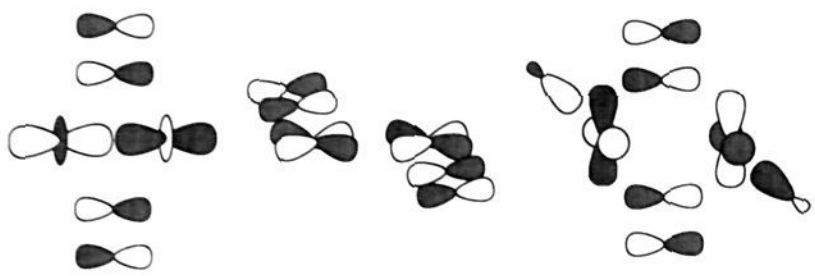

Figure 9. Frontier molecular orbitals of **1**, obtained from Fenske–Hall calculations (ref 21). Fe atoms and bridging carbonyl ligands lie in the plane of the page (yz), and terminal carbonyls are perpendicular to it.

carbonyl ligand. Thus, the resonance Raman results can help in painting a picture of the changes in the metal–carbonyl interaction.

The excitation profiles indicate that, relative to the ground state, excitation into the first absorption band has a greater effect on the terminal C–O bonds than on the bridging C–O bonds. Likewise, the second absorption band corresponds to an ES in which there are greater changes in the bridging C–O bonds. Although we are aware of the difficulties of interpreting electronic spectra via molecular orbital theory, we believe that these results are qualitatively explained by a consideration of the characters of the frontier MO's of **1**,[21] calculated via the approximate Fenske–Hall molecular orbital method.[22]

We shall consider the trans isomer **1t**, oriented so that the 2-fold axis coincides with the z axis and the y axis goes through the Fe atoms.[23] In this coordinate system, the Fe $3d_{xz}$ and $3d_{xy}$ orbitals are oriented to interact strongly with the 2π orbitals of the terminal CO's. The Fe–Fe σ interaction involves the $3d_{y^2}$ AO's, which are orthogonal to the 2π orbitals of the terminal carbonyls. The second-highest occupied MO (SHOMO), HOMO, and LUMO of **1t** are sketched in Figure 9.

The HOMO can be roughly described as an Fe–Fe π^* interaction involving the $3d_{xy}$ AO's, stabilized via backbonding to the terminal CO ligands. The LUMO is predominantly Fe–Fe σ^* in character, with small contributions from the 2π orbitals of the bridging carbonyls. If the lowest-energy optical transition in **1t** corresponds roughly to a one-electron transition from the HOMO to the LUMO, the orbital characters indicate that the terminal CO ligands should be more greatly affected than the bridging CO's, consistent with the excitation profiles. Further, the HOMO-LUMO transition will weaken the Fe–Fe bond and will have little effect on the Fe–CO bonds. This observation seems consistent with the observation that low-energy excitation can cause homolysis of the Fe–Fe bond but not CO loss.[3i,4a,g,h]

The SHOMO of **1t** involves the Fe $3d_{z^2-y^2}$ AO's, stabilized by interaction with the 2π orbitals of the bridging CO's and the 5σ orbitals of the terminal CO's. An excitation from this MO to the LUMO will have a much larger effect on the bridging CO bonds than on the terminal ones. The excitation profiles show that excitation into the second absorption band induces a much greater intensity enhancement for the bridging CO's than the terminal CO's, which would be consistent with a SHOMO/LUMO transition.

(21) Bursten, B. E.; Cayton, R. H. *J. Am. Chem. Soc.* **1986**, *108*, 8241–9.

(22) Hall, M. B.; Fenske, R. F. *Inorg. Chem.* **1972**, *11*, 768–75.

(23) In discussing the electronic structure of **1** or **1***, recall that the terminal carbonyls are roughly perpendicular to the line connecting the Fe atoms and to the plane defined by the Fe atoms and the bridging carbonyls: (a) Bryan, R. F.; Greene, P. T. *J. Chem. Soc. A* **1970**, 3064–8. (b) Bryan, R. F.; Greene, P. T.; Newlands, M. J.; Field, D. S. *J. Chem. Soc. A* **1970**, 3068–74.

We are aware that the correlation of the MO characters with the excitation profiles is approximate at best. Nevertheless, the qualitative agreement is satisfying. We are currently exploring a better relationship between the density changes in the excitations and the excitation profiles via ab initio calculations on these systems.

Low-Energy Vibrations. The origin of the Raman peaks observed in the lower of the energy ranges examined (Figures 5 and 6) can be readily identified by reference to the earlier discussion of the CO stretches. Those peaks that appear in the off-resonance spectra (λ_{irr} = 648 nm) and whose intensity appears to depend linearly on irradiation power can be assigned to vibrations of **1** or **1***. Vibrational modes of **2** or **2*** are responsible for those bands that exhibit intensity enhancement at irradiation wavelengths of 528.7, 514.5, and 457.9 nm and that show a nonlinear dependence on photon density. The positions of all the observed low-energy bands are reported in Table 2.

The lowest-energy vibrational mode detected in the off-resonance spectrum of **1**, at 225 cm^{-1}, had already been observed in solid samples[9] and was assigned, by comparison with similar compounds, to the Fe–Fe stretching mode. It is also the dominant lowest energy band at λ_{irr} = 351 nm and is observed as a shoulder on the more intense 214 cm^{-1} peak of **2** when λ_{irr} = 514.5 or 457.9 nm. The weak Raman bands at 348 and 403 cm^{-1} show no intensity enhancement in the first absorption band, and they may be due to Cp ring bends.[24] On the other hand, the 440 cm^{-1} peak which, among the spectra presented here, is only visible in the 514.5 nm data, is at the appropriate energy to be the resonance enhanced second overtone of the Fe–Fe stretch. Shorter wavelength irradiation, e.g. 351 or 263 nm, yields spectra dominated by new, broad, and intense features that are also likely associated with the Cp or Cp* ligands of **1** or **1***.

A comparison of the spectra of **1** and **1*** (Figures 5 and 6) is both interesting and complex. As noted above, the 648 nm spectrum of **1** shows a sharp band at 225 cm^{-1}, which we ascribe predominantly to the Fe–Fe stretching mode. The lowest energy band in the 514.5 nm spectrum of **1** is noticeably shifted to 214 cm^{-1}, reflecting the Fe–Fe stretching mode in **2**. By contrast, the lowest energy band in both the 648 and 514.5 nm spectra of **1*** occurs at 140 cm^{-1}, although there is a shoulder on the high-energy side of the band for λ_{irr} = 648 nm, at about 154 cm^{-1}. Other bands present in the 514.5 nm spectrum of **1*** are also seen in the 648 nm spectrum, albeit at greatly reduced intensity. Because the bands in the 514.5 nm spectrum of **1*** are mostly due to photogenerated **2***, it seems apparent that bands of **2*** are present in the off-resonance 648 nm spectrum. To ascertain whether the 648 nm irradiation wavelength was indeed off-resonance, and to make sure that no shorter wavelength light from the argon ion pump laser was arriving to the sample, data were also collected with 785 nm light, with identical results. At this point, the possibility of multiphoton processes generating the CO-loss product **2***, which has a long enough half-life to accumulate and be detected even under these unfavorable conditions, cannot be ruled out.

The lowest energy Raman band of **1***, with a frequency in the range 154–140 cm^{-1}, is most likely attibuted primarily to the Fe–Fe stretching mode. This vibrational frequency is significantly lower than the same mode in **1**, which is observed at 225 cm^{-1}. This difference is curious in light of the similarity in the Fe–Fe distances in **1** and **1***.[25] We believe that the lower Fe–Fe stretching frequency in **1*** relative to **1** is due in large

(24) Fritz, H. P. *Adv. Organomet. Chem.* **1964**, *1*, 239.

(25) Teller, R. G.; Williams, J. W. *Inorg. Chem.* **1980**, *19*, 2770–3.

part to the coupling of the heavier Cp* ligands with the iron atoms, which increases the effective reduced mass for this vibrational mode, rather than to a specific electronic structural difference between the molecules.

Because of the strong intensity of the spectra of **2** and **2*** at $\lambda_{in} = 528.7$ and 514.5 nm, it is not possible to obtain excitation profiles for the low-energy bands of **1** and **1*** like those of Figure 4 for the CO stretches. However, it is evident from Figure 5 that the 225 cm^{-1} peak is undergoing a very modest, at best, resonance enhancement. Such behavior is quite unlike that of the carbonyl stretching modes, but can be understood in view of the supposed Fe−Fe dissociative nature of the ES reached by irradiation into the first or second absorption band. In particular, the time-dependent theory of light-matter interaction[11,26] indicates that the presence of a dissociative mode would cause fast wavepacket propagation damping, which implies that short-time dynamics would dominate absorption and scattering phenomena. Under such conditions, the intensity enhancement of Raman bands due to low-energy modes tends to decrease relative to those of high-energy vibrations, just in the way observed for **1** and **1***. Moreover, short-time-limit behavior is characterized by broad, featureless absorption spectra, which is consistent with the observed lack of structure observed even in the 77 K spectrum of **1**.[3b]

In general, the intensity of Raman bands is proportional to the square of the distortion of the ES equilibrium position with respect to the GS, Δ^2. However, in the short-time limit, it becomes proportional to $\Delta^2\omega^2$, where ω is the vibrational frequency, i.e. to the square of the slope of the potential energy surface of ES along that normal coordinate at the GS equilibrium geometry. This relation supports the validity of our analysis of the excitation profiles of the CO stretches as being related to the initial distortion of the molecule upon photolysis and, ultimately, to the photochemical activity.

Perhaps the most striking feature of the low-energy Raman spectra of **1** and **1*** is the observation of intense and detailed spectra of the CO-loss intermediates **2** and **2***, certainly a rare occurrence for transient species in solution. Figures 7 and 8 present the 514.5 nm spectra of **1** and **1*** in which the peaks that show linear intensity dependence have been factored out. As such, all the peaks should result from transients **2** and **2***, with no interference from **1** and **1***. Both spectra show two rich Franck−Condon progressions, each based on the totally-symmetric lowest-energy vibrational mode. For **2**, the fundamentals are at 214 and 514 cm^{-1}, with successive excitations of 214 cm^{-1} forming the progressions. The peak at 300 cm^{-1} is due to the difference between the fundamentals, and must originate from a hot band. The fundamentals for **2*** are 142 and 528 cm^{-1}, and the spectrum remarkably shows up to the sixth overtone of the 142 cm^{-1} fundamental. In both cases, the anharmonicity of the lower-energy mode appears to be smaller than the experimental precision. The small anharmonicity, together with the number of overtones and combination bands and the overall intensity of the spectra, indicates that **2** and **2*** are very photostable with respect to dissociation at this excitation wavelength. A dissociative mode, as seen in the case of **1** and **1***, would dramatically affect the Raman scattering of the low-energy modes of **2** and **2***. We can therefore rule out the possibility that the radical formation from **1** and **1***, observed at low photon energies, proceeds via intermediates **2** or **2***. These results support the existence of two separate initial photodissociation pathways.

(26) (a) Lee, S.-Y.; Heller, E. J. *J. Chem. Phys.* **1979**, *71*, 4777−88. (b) Heller, E. J. *Acc. Chem. Res.* **1981**, *14*, 368−75. (c) Heller, E. J.; Sundberg, R. L.; Tannor, D. *J. Phys. Chem.* **1982**, *86*, 1822−33. (d) Tannor, D. J.; Heller, E. J. *J. Chem. Phys.* **1982**, *77*, 202−18.

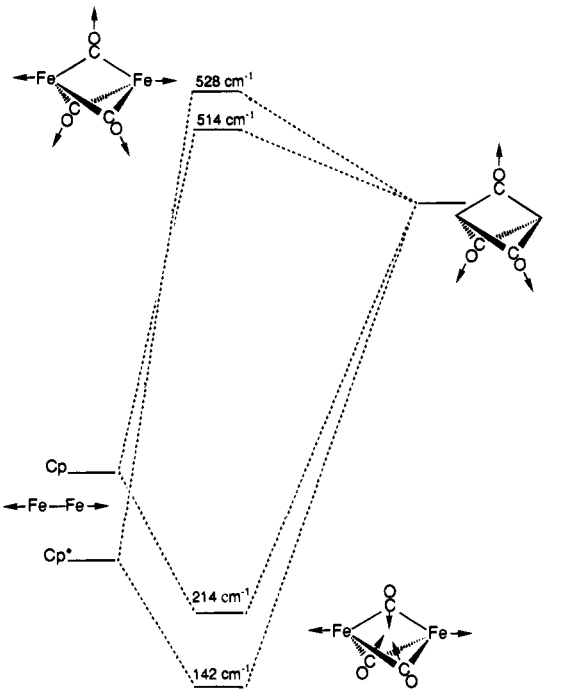

Figure 10. Qualitative representation of the low-energy vibrational normal modes of **2** and **2***. The hypothetical "pure" Fe−Fe stretch and Fe−C breathing modes are depicted on the left and right sides of the diagram; their observed low- and high-energy combinations are shown in the center.

The observation of two fundamental modes for **2** and **2*** is reasonable given the structure of the $Fe_2(\mu\text{-}CO)_3$ core of these molecules. This core is expected to have two low-energy totally-symmetric (A_1' under D_{3h} symmetry) vibrational modes, namely the Fe−Fe stretch and the Fe−C "breathing" mode (Figure 10). Two A_1' normal modes will result from the coupling of these fundamentals. In the lower energy normal mode, the carbon atoms move inward as the Fe atoms move apart, thus minimizing the stretching of the Fe−C bonds. In the higher energy mode, the carbon atoms move outward as the Fe atoms move apart, necessarily stretching the Fe−C bonds as well as the Fe−Fe bond. The coincident resonance enhancement of the 214 and 514 cm^{-1} and of the 142 and 528 cm^{-1} fundamentals in the spectra of **2** and **2***, respectively, and the intensity of their combination bands strongly suggest that they indeed correspond to the normal modes just described.

Strong coupling between the Fe−Fe and Fe−C stretches within the core of **2** and **2*** would also help explain the surprising near identity of the lowest energy Raman bands of **1** and **2** and of **1*** and **2***. According to the effective atomic number rule, complexes **1** and **1*** have Fe−Fe single bonds whereas **2** and **2*** possess Fe−Fe double bonds. Based on this simple analysis, one would expect the Fe−Fe stretching frequencies of **2** and **2*** to be significantly higher than those in **1** and **1***, respectively. We propose that the contribution of the bridging carbonyls to the lowest-energy normal mode is far more significant in **2** and **2*** than it is in **1** and **1***. Significant mixing of the carbonyls would depress the apparent energy of the Fe−Fe stretching mode to a value lower than that of a "pure" Fe−Fe double bond,[27] and, in fact, closer to the value observed for an Fe−Fe single bond.

The higher energy normal mode in **2*** is at higher frequency than that in **2**. This somewhat surprising result could be due to the mixing of another low-energy totally symmetric mode, namely the $C-CH_3$ deformation of the Cp* ligands. This

(27) Kubas, G. J.; Spiro, T. G. *Inorg. Chem.* **1973**, *12*, 1797−801.

explanation has been used to interpret the vibrational spectra of Cp^*_2M systems.[28]

One remarkable difference between the spectra of **2** and **2*** in Figures 7 and 8 lies in the intensity distribution of the overtones of the lower energy vibration. For **2**, the fundamental is the most intense band. However, in the spectrum of **2***, both the second and third overtones are more intense than the fundamental, the third overtone being the most intense. The transform approach to resonance Raman helps understanding such difference.[11,29] According to this method, the intensity of a fundamental resonance Raman band is proportional to Δ^2, the square of the ES distortion, the intensity of the second overtone to Δ^4, and so on. The other factors that affect the relative intensities of the overtones are the absorption cross section and the shape of the electronic absorption band of the particular ES. Unfortunately, only difference transient absorption spectra or low-temperature matrix spectra are available for these intermediates. It is, therefore, impossible to calculate exactly the Δ's. However, because the transient absorption spectra of **2** and **2*** are extremely similar, it is likely that the different intensity ratio of fundamental and overtones for the lower energy vibration of **2** and **2*** derives from a difference in the distortion of their ES along the normal coordinate. Precisely, larger overtone intensity suggests that the Cp* intermediate **2*** should have a larger distortion along the coordinate, which we have identified as the low-energy combination of Fe−Fe stretch and CO bridge "breathing". This result seems consistent with the lower frequency that this mode presents in **2*** than in **2**, and indicates a more easily distorted Fe−Fe bond.

Finally, as already pointed out, the observation of such intense spectra of unstable species is the result of a number of concomitant factors: the long half-life of these intermediates, the relatively high efficiency of their formation at these wavelengths and, especially, a very intense electronic absorption band yielding very large resonance enhancement. However, it should be noticed that the intensity of the Raman spectrum of **2** and **2*** follows a different irradiation wavelength dependence in the low-energy range than it does for the carbonyl stretch. Specifically, their carbonyl stretching vibration is most intense with λ_{irr} = 457.9 nm (Figure 4), whereas the intensity of the low-energy bands clearly decreases in going from the 514.5 nm to the 457.9 nm spectrum. Resonance enhancement is expected to be greatest at 514.5 nm, which is almost at the maximum of the electronic absorption band of either **2** or **2***; on the other hand, the efficiency of formation of the CO-loss intermediates should increase with increasing irradiation energy. It is clear, therefore, that the C−O stretch of **2** or **2*** is not strongly coupled to the electronic transition responsible for the 510 nm absorption band, which, in turn, must involve a large change in the bonding relationship within the $Fe_2(\mu\text{-}C)_3$ core.

(28) Bandy, J. A.; Cloke, F. G. N.; Cooper, G.; Day, J. P.; Girling, R. B.; Graham, R. G.; Green, J. C.; Grinter, R.; Perutz, R. N. *J. Am. Chem. Soc.* **1988**, *110*, 5039−5050.

(29) Blazej, D. C.; Peticolas, W. L. *J. Chem. Phys.* **1980**, *72*, 3134−42.

Conclusion

We have shown that Raman spectroscopy of dinuclear organometallic complexes can yield valuable vibrational data for both high-energy vibrations, such as carbonyl stretches, and low-energy vibrations, such as metal−metal stretches. Because Raman spectroscopy necessarily involves the coupling of vibrational and electronic excitations, it provides a wealth of information about the interrelationship between molecular vibrations and molecular electronic structure. We are quite frankly surprised that so few Raman studies of dinuclear complexes have been undertaken, and we believe that the present results will stimulate further investigations.

We have also shown that the Raman experiment can be used for the *in situ* generation and detailed spectroscopic probing of photochemical transient species of organometallics. The first direct observation of high- and low-energy vibrations of organometallic transients, including vibrational progressions, is startling, especially given the multitude of studies of these molecules by other spectroscopic methods. We believe that this exciting result demonstrates that Raman spectroscopy will become a major tool in the study of the photochemical dynamics of organometallic molecules.

Acknowledgment. We gratefully acknowledge the National Science Foundation (Grant CHE-9208703 to B.E.B., and Instrumentation Grant CHE-9108384 to T.L.G. and B.E.B.), the Ohio State University Center for Materials Research (T.L.G.), and the National Institutes of Health (Grant AR38917 to R.H.) for support of this research.

JA9432168